Control Strategy for Improved Dynamic Performance of Variable-speed Drives with the Modular Multilevel Converter

Jae-Jung Jung, Hak-Jun Lee, *Student Member*, *IEEE*, and Seung-Ki Sul, *Fellow*, *IEEE*
School of Electrical & Computer Engineering
Seoul National University
Seoul, Korea
Email: jaejung.jung@eepel.snu.ac.kr

***Abstract*—This paper presents a control scheme for the Modular Multilevel Converter (MMC) to drive a variable-speed AC machine, especially focusing on improving dynamic performance. Theoretically, the energy balance in the cell capacitors is prone to be unstable at startup and low frequency operation. Therefore, the MMC topology essentially requires advanced strategies for energy balancing so as to suppress the voltage pulsation of each cell capacitor. The pulsation is getting larger as the output frequency of MMC is getting lower. This paper proposes a strategy for robust dynamic response even at zero output frequency of MMC employing leg offset voltage injection. With this proposed strategy, an AC machine has been driven from standstill to rated speed without excessive cell capacitor voltage ripples. The experimental results verify that stable operation is guaranteed for both a 15r/min operation with 40% step load torque and the entire frequency operation with varying load torque.**

Keywords—modular multilevel converter; motor drive; inner circulating current; arm energy balancing; dynamic performance

NOMENCLATURE

Superscript '*'	reference value.
Superscript '~'	low frequency component.
Superscript '^'	high frequency component.
x-phase	representation for one of *u, v,* or *w* phases.
v_{xo}	leg offset voltage of *x*-phase leg.
v_{sn}	common mode voltage.
i_{xo}	circulating current of *x*-phase leg.
ω_s	three-phase output frequency.
R	resistance of arm inductor.
L	inductance of arm inductor.
C_{cell}	capacitance of DC capacitor in a sub-module cell.
E_{xP}	upper arm energy in *x*-phase leg.
E_{xN}	lower arm energy in *x*-phase leg.
v_{xPi}^{C}	i^{th} cell capacitor voltage in upper arm in *x*-phase.
v_{xNi}^{C}	i^{th} cell capacitor voltage in lower arm in *x*-phase.

I. INTRODUCTION

A Modular Multilevel Converter (MMC) has been discussed with a focus on high-power medium voltage AC motor drives [1]-[10]. The use of the MMC makes it possible to save bulky reactive components in a medium-voltage motor drive application such as line-transformer, harmonic filter, and DC-link reactor. Compared to conventional medium voltage source converters, the MMC has modular structure which is made up of identical converter cells. Because it can easily provide higher number of voltage level for medium voltage application, the quality of the output voltage waveform would be better. Also, because of the modular structure it has advantages such as easy maintenance and assembly.

Fig. 1 shows the circuit configuration of an MMC. This topology needs to be controlled by extra balancing strategies. As shown in Fig. 1, since the upper and lower arm currents flow through cells in each arm, the corresponding arm currents cause fundamental periodic pulsations of cell capacitor voltages. Theoretically, the voltage pulsation of the capacitor of each cell is proportional to output phase current and inversely proportional to operating frequency [6]. For this reason, the special effort is demanded to drive AC machine by MMC, that requires a starting torque and low speed steady state operation. In the recent studies [7]-[9], principles and algorithms for AC motor drives with the MMC have been introduced. But they do not address the actual control strategies such as changing output frequency including standstill and varying load torque. Especially, the authors in [8] provided no experimental verification for any three-phase machine. Moreover, compared to the circulating current injection method in [7] and [9]-[10], the proposed method in this study does directly produce the leg offset voltage reference for controlling circulating currents. From the perspective of the control dynamics and control complexity, the leg offset voltage injection method is better and simpler than the circulating current injection method.

In summary, the goal of this paper is proposing a control strategy of the entire frequency range operation including standstill for variable speed AC motor drive. In addition, the proposed method is devised to reduce the degradation of the control performance of MMC when the load torque changes abruptly. The control scheme introduces two operation modes. One is a low frequency mode for startup and low speed

operation, and the other is a normal frequency mode from medium to higher speed operation. The strategy in the low frequency mode exploits a leg offset voltage and a common mode voltage with high frequency component to suppress the voltage ripple of the cell capacitor. The square wave voltage is used as the leg offset voltage, which reduces the peak of circulating current compared to sinusoidal waveform of the voltage [7]. And, a switchover tactic between two operation modes is described to drive AC machine in overall speed region.

Finally, experiments for variable-speed AC motor drives by a 10kVA prototype MMC emulating fans, blowers, or pump drive system were performed to verify the feasibility of the proposed balancing strategy. First, the experiments were conducted for comparing features of the sinusoidal and square wave leg offset voltage. Second, for verifying dynamic performance, the stable operation at 1Hz operation is demonstrated under an abrupt step load torque from 0% to 40%. Lastly, the experimental results show that all control strategies is well implemented and incorporated properly by driving variable-speed AC motor with a load where the torque varies in proportional to the square of the speed, similar to fans, blowers, or pumps.

II. CONFIGURATION AND BASIC PRINCIPLE OF THE MMC

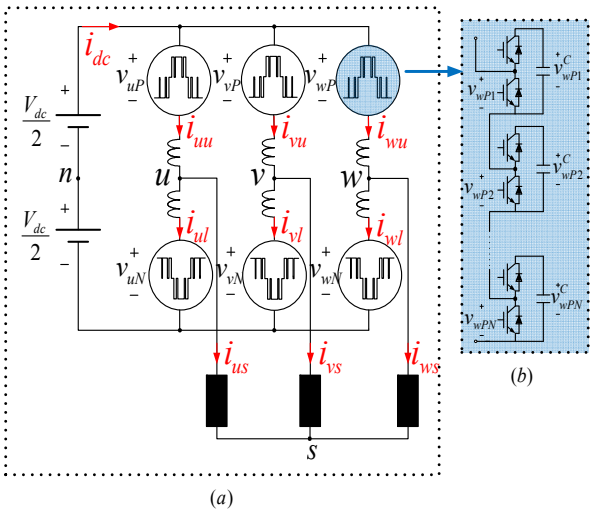

Fig. 1. Circuit configuration of the MMC.

Fig. 1(a) shows the circuit configuration of the MMC. The three-phase MMC is composed of three legs. Each leg has two arms and two arm inductors. Each arm has cascaded N-identical half-bridge circuit based cells, and each cell consists of one DC capacitor and two active switching devices. The cascaded cell modules are depicted in Fig. 1(b) in detail. In Fig. 1(a), first, i_{xu} and i_{xl} are the upper and lower arm currents, respectively, and i_{xs} is the output phase current, where the notation 'x' represents u, v, or w phase. The output phase current, i_{xs}, and circulating current, i_{xo}, are calculated from the upper and lower arm currents as described in (1)-(2). Therefore, the arm currents can be deduced as (3)-(4), according to decoupled control scheme in [8], [11].

$$i_{xs} = i_{xu} - i_{xl} . \tag{1}$$

$$i_{xo} = (i_{xu} + i_{xl}) / 2 . \tag{2}$$

$$i_{xu} = \frac{1}{2} i_{xs} + i_{xo} . \tag{3}$$

$$i_{xl} = -\frac{1}{2} i_{xs} + i_{xo} . \tag{4}$$

The leg offset voltage, v_{xo}, to produce a circulating current is defined as (5), where R and L are resistance and inductance of an arm inductor assuming that all arm inductors in MMC are identical. From the voltage relationships along x-phase loop, the upper and lower arm voltage reference are respectively denoted as (6) and (7) where V_{dc} is DC-link voltage, v_{xP} and v_{xN} are the upper and lower arm voltages, respectively. The common mode voltage, v_{sn}, is voltage difference between node 's' and node 'n', and v_{xs} is the phase voltage which is $v_{xs} = V_m cos\,(\omega_s t)$. In addition, the superscript "$*$" refers to the corresponding term for the reference values. A detailed mathematical description for the relationships in an MMC is done in [10].

$$v_{xo} = (R + L\frac{d}{dt}) i_{xo} . \tag{5}$$

$$v_{xP}^{*} = \frac{V_{dc}}{2} - v_{xs}^{*} - v_{sn}^{*} - v_{xo}^{*} . \tag{6}$$

$$v_{xN}^{*} = \frac{V_{dc}}{2} + v_{xs}^{*} + v_{sn}^{*} - v_{xo}^{*} . \tag{7}$$

The instantaneous power of each arm in x-phase can be deduced as (8)-(9), and these two equations have to be considered for understanding the proposed balancing control.

$$P_{xP} = v_{xP}^{*} i_{xu} = \left(\frac{V_{dc}}{2} - v_{xs}^{*} - v_{sn}^{*} - v_{xo}^{*} \right) \left(\frac{i_{xs}}{2} + i_{xo} \right) . \tag{8}$$

$$P_{xN} = v_{xN}^{*} i_{xl} = \left(\frac{V_{dc}}{2} + v_{xs}^{*} + v_{sn}^{*} - v_{xo}^{*} \right) \left(-\frac{i_{xs}}{2} + i_{xo} \right) . \tag{9}$$

In addition, the upper and lower arm energy can be calculated as (10) and (11), respectively. Each arm energy is the sum of the cell capacitor energies in corresponding arm at x-phase leg.

$$E_{xP} = \frac{1}{2} C_{cell} \sum_{i=1}^{N} (v_{xPi}^{C})^2 . \tag{10}$$

$$E_{xN} = \frac{1}{2} C_{cell} \sum_{i=1}^{N} (v_{xNi}^{C})^2 . \tag{11}$$

III. PROPOSED BALANCING CONTROL SCHEMES

A. Startup and Low Frequency Mode

The capacitor power difference between the upper and lower arm, which is derived as (12) from (8) and (9), affects balance of cell capacitor voltage of arms. The first term of the right-hand side in (12), $0.5V_{dc}i_{xs}$, has fundamental frequency component. Thus, when output frequency is DC or very low, the voltage difference between arms would diverge due to this low frequency power term.

$$P_{xP} - P_{xN} \approx 0.5V_{dc}i_{xs} - 2v_{xs}^{*}i_{xo} - 2v_{sn}^{*}i_{xo} - v_{xo}^{*}i_{xs} . \quad (12)$$

To balance the power difference between arms, a control strategy exploiting common mode voltage, v_{sn}, was used in this paper. The common mode voltage can be regarded as an additional degree of freedom for controllability because the common mode voltage does not affect to the line-to-line output voltage. It is natural to select the frequency of the common mode voltage as a high frequency to minimize the fluctuation of the cell capacitor voltage. In addition, since circulating current, i_{xo}, is also controllable element that does not affect the output phase current, high frequency component can be superimposed on circulating current. Hence, the third term of the right-hand side in (12), $2v_{sn}^{*}i_{xo}$ can be used for the balance of power of arms with high frequency component in v_{sn} and i_{xo}. For convenience, the low and high frequency elements can be segregated from i_{xo} and v_{sn} as (13) and (14), where "~" and "^" mean low and high frequency component respectively.

$$i_{xo} = \tilde{i}_{xo} + \hat{i}_{xo} . \quad (13)$$

$$v_{sn} = \hat{v}_{sn} . \quad (14)$$

The difference in power between upper and lower arm can be rearranged from (12)-(14), and then, the low frequency power component can be extracted like (15). Here, the power difference should be controlled to be null.

$$P_{xP} - P_{xN}\big|_{low\ freq.} \approx \frac{1}{2}V_{dc}i_{xs} - 2v_{xs}^{*}\tilde{i}_{xo} - 2\hat{v}_{sn}^{*}\hat{i}_{xo}^{*}\Big|_{low\ freq.} = 0 . \quad (15)$$

To nullify the low frequency power component like (15), the low frequency component of $2\hat{v}_{sn}^{*}\hat{i}_{xo}^{*}$ can be controlled. Thus, $\hat{v}_{sn}^{*}$ and $\hat{i}_{xo}^{*}$ should be regulated as the same high frequency to make the power term of $2\hat{v}_{sn}^{*}\hat{i}_{xo}^{*}$ have DC or low frequency component.

In the case of the sinusoidal leg offset voltage injection method, $\hat{v}_{sn}^{*}$ and $\hat{v}_{xo}^{*}$ can be defined by (16)-(17), and ω_h stands for the angular speed of high frequency component, V_{sn} for the effective value of common mode voltage, and $\tilde{V}_{xo}$ for the magnitude of high frequency leg offset voltage which may have DC and several low frequency components.

$$\hat{v}_{sn}^{*} = \sqrt{2}V_{sn}\cos(\omega_h t) . \quad (16)$$

$$\hat{v}_{xo}^{*} = \tilde{V}_{xo}\cos(\omega_h t + \phi) . \quad (17)$$

The phase angle ϕ in (17) between the leg offset voltage and circulating current is derived from (18) to make the circulating current be synchronized with common mode voltage.

$$\phi = \arctan(\frac{\omega_h L}{R}) . \quad (18)$$

Under the assumption of $R \ll \omega_h L$, ϕ is approximated to $\pi/2$. From (5) and (16)-(17), the low frequency component of the power associated with the common mode voltage and the circulating current can be derived as (19) using the leg offset voltage, which p is the differential operation.

$$\begin{aligned} 2\hat{v}_{sn}\hat{i}_{xo}\big|_{low\ freq.} &\approx 2\hat{v}_{sn}\frac{\hat{v}_{xo}}{pL}\Big|_{low\ freq.} \\ &= \frac{2\sqrt{2}V_{sn}\tilde{V}_{xo}}{\omega_h L}\cos(\omega_h t)\sin(\omega_h t + \frac{\pi}{2})\Big|_{low\ freq.} \\ &= \frac{2\sqrt{2}V_{sn}\tilde{V}_{xo}}{\omega_h L}\left(\frac{1}{2}\sin(\frac{\pi}{2}) + \frac{1}{2}\sin(2\omega_h t + \frac{\pi}{2})\right)\Big|_{low\ freq.} \\ &= \frac{\sqrt{2}V_{sn}\tilde{V}_{xo}}{\omega_h L} . \end{aligned} \quad (19)$$

And then, $2\hat{v}_{sn}^{*}\hat{i}_{xo}^{*}$ in (15) can be substituted with (19). So, the magnitude of high frequency leg offset voltage, $\tilde{V}_{xo}$, can be calculated as (20).

$$\begin{aligned} &\frac{\sqrt{2}V_{sn}\tilde{V}_{xo}}{\omega_h L} = \frac{1}{2}V_{dc}i_{xs} - 2v_{xs}^{*}\tilde{i}_{xo} \\ &\Leftrightarrow \tilde{V}_{xo} \approx \frac{\omega_h L}{\sqrt{2}V_{sn}}\left(\frac{1}{2}V_{dc}i_{xs} - 2v_{xs}^{*}\tilde{i}_{xo}\right). \end{aligned} \quad (20)$$

In the case that the sinusoidal wave voltage is injected to both the common mode and the leg offset voltage, the balancing control strategy is depicted as a block diagram in Fig. 2(a).

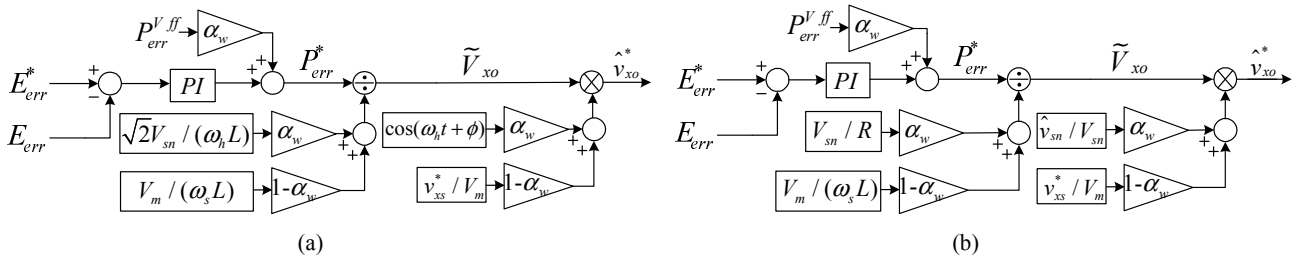

Fig. 2. Proposed control scheme for variable-speed drives: (a) sinusoidal wave voltage injection method, (b) square wave voltage injection method. α_W is weighting factor for switchover, which is described in section *C* of chapter III.

Here, E_{err} is the difference in energy between upper and lower arm as (21). E_{err}^{*} is the reference of energy difference, and should be set as null to keep the balance of the arm energies.

$$E_{err} = E_{xP} - E_{xN} = \frac{1}{2} C_{cell} \left\{ \sum_{i=1}^{N} (v_{xPi}^{C})^2 - \sum_{i=1}^{N} (v_{xNi}^{C})^2 \right\}. \quad (21)$$

And $P_{err}^{V\_ff}$ in Fig. 2(a) can be derived as (22) by (20).

$$P_{err}^{V\_ff} = \frac{1}{2} V_{dc} i_{xs} - 2 v_{xs}^{*} \tilde{i}_{xo}. \quad (22)$$

In the case of the square leg offset voltage injection, on the other hand, the square wave voltage can be injected to both the common mode and the leg offset voltage as shown in Fig. 2(b). In that case, $\hat{v}_{sn}^{*}$ can be defined by (23), and f_h stands for the frequency of the injected high frequency voltage.

$$\hat{v}_{sn}^{*} = \begin{cases} -V_{sn} & (0 \le t < \frac{1}{2f_h}) \\ V_{sn} & (\frac{1}{2f_h} \le t < \frac{1}{f_h}) \end{cases}. \quad (23)$$

Under the assumption that the arm resistance, R, is dominant during each given quasi steady half period, $1/(2f_h)$, $\hat{v}_{xo}^{*}$ can be approximated as (24) from (5), (15), and (23).

$$\hat{v}_{xo}^{*} \approx \begin{cases} -\frac{R}{2V_{sn}} \left(\frac{1}{2} V_{dc} i_{xs} - 2 v_{xs}^{*} \tilde{i}_{xo} \right) & (0 \le t < \frac{1}{2f_h}) \\ \frac{R}{2V_{sn}} \left(\frac{1}{2} V_{dc} i_{xs} - 2 v_{xs}^{*} \tilde{i}_{xo} \right) & (\frac{1}{2f_h} \le t < \frac{1}{f_h}) \end{cases}. \quad (24)$$

And $P_{err}^{V\_ff}$ in Fig. 2(b) can also be derived from (22) by using (24) similarly with the case of sinusoidal wave.

B. Normal Frequency Mode

In normal frequency mode, since the output frequency is high enough, the voltage fluctuation of the cell capacitor is tolerable. And, in this mode, the circulating current is controlled to have only DC component to minimize the conduction loss caused by the additional circulating current. As the operation frequency increases, meanwhile, the margin of the common mode voltage decreases. Hence, the common mode voltage is less available for balancing control.

The practical MMC systems may have an inherent unbalance owing to slight asymmetries in cells, structural errors, and others. In normal frequency mode, therefore, it should be performed just to eliminate the inevitable small DC unbalance. The balancing can be achieved by using the circulating current as $2v_{xs}^{*}i_{xo}$ in (12). By regulating the leg offset voltage for circulating current to have fundamental frequency component, this DC unbalance can be suppressed.

C. Switchover between Two Modes

As mentioned before, because the high frequency components of the common mode and leg offset voltage is only injected in low operating frequency mode, the leg offset voltage reference is changed depending on the output frequency of MMC. A switchover tactic between low and high frequency modes shown in Fig. 3 is devised by weighting factor, α_W. And, this factor is applied to switchover of balancing control diagram as shown in Fig. 2. In addition, the tactic would have the hysteresis band to prevent chattering in the vicinity of switchover frequency, f_{cut}.

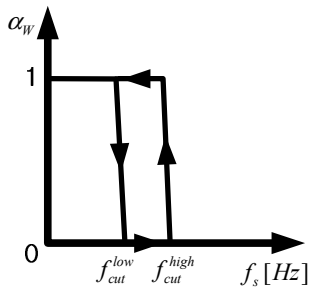

Fig. 3. The relationship between operating frequency and weighting factor.

IV. Overall Control Scheme for Entire Frequency Operation

Fig. 4 shows the overall controller for the entire frequency operation from the standstill to normal frequency mode.

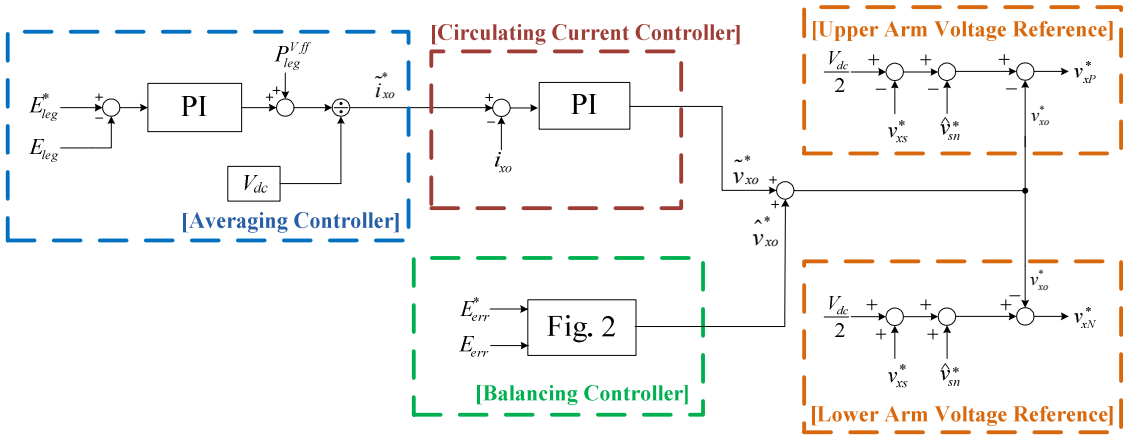

Fig. 4. Proposed overall control scheme for variable-speed drives.

First, the averaging controller carries out regulating the leg power which means difference between input power from DC-link and AC output power. The leg power is calculated as (25) by sum of (8) and (9).

$$P_{xP} + P_{xN} \approx V_{dc}\tilde{i}_{xo} - 2v_{xo}^{*}\hat{i}_{xo} - v_{xs}^{*}i_{xs} - \hat{v}_{sn}^{*}i_{xs}\,. \quad (25)$$

The low frequency power component in (25) should be controlled to be null like (26), so the output of the controller has DC and 2nd order harmonic frequency components as described like (27).

$$P_{xP} + P_{xN}\big|_{low\ freq.} = V_{dc}\tilde{i}_{xo}^{*} - v_{xs}^{*}i_{xs} = 0\,. \quad (26)$$

$$\tilde{i}_{xo}^{*} = \frac{v_{xs}^{*}i_{xs}}{V_{dc}}\,. \quad (27)$$

E_{leg} is the energy of the leg, and it can be calculated as (28). E_{leg}^{*} is the reference energy of the leg as (29), where v_c^{*} is the reference value of cell capacitor voltage, which is V_{dc}/N.

$$E_{leg} = E_{xP} + E_{xN} = \frac{1}{2}C_{cell}\sum_{i=1}^{N}\left\{\left(v_{xPi}^{C}\right)^{2} + \left(v_{xNi}^{C}\right)^{2}\right\}. \quad (28)$$

$$E_{leg}^{*} = \frac{1}{2}\frac{C_{cell}}{2N}4N^{2}v_{c}^{*2} = NC_{cell}v_{c}^{*2}\,. \quad (29)$$

The feed-forwarding power term, P_{leg}^{Vff}, is derived as $v_{xs}^{*}i_{xs}$ from (27). Therefore, the proportional and integral controller can simply be adopted as the circulating current controller for the averaging control. The details about the averaging controller are described in [10].

Meanwhile, the balancing controller can be chosen between two algorithms in Fig. 2 which are the sinusoidal and the square wave voltage injections. As shown like Fig. 4, the balancing controller directly makes the leg offset voltage without the circulating current controller for eliminating energy difference between upper and lower arms. By reason of this fact, the balancing controller has a wider bandwidth, and can achieve a good transient response.

Finally, the upper and lower arm voltage references are synthesized as (6) and (7), which are composed of v_{xs}^{*} from the output of phase current controller, v_{xo}^{*} from the averaging and the balancing controller, and the injected common mode voltage of $\hat{v}_{sn}^{*}$.

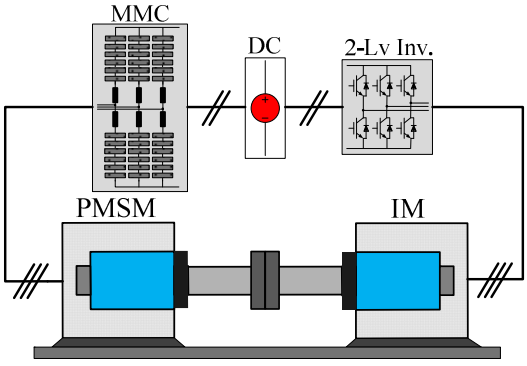

Fig. 5. Experimental setup with 300V 10kVA prototype MMC system.

V. Experimental Results

The proposed control scheme was validated by the 300V 10kVA prototype MMC in Fig. 5. The number of cells in each arm, *N*, equals 6. Thus, total 36 cells are used for three-phase system. Each cell capacitor voltage was controlled to be 50V. The level-shifted Phase Disposition PWM (PD-PWM) is applied to generate arm voltage references [12]-[13]. The switching frequency of each cell is set as 2kHz and the capacitance of DC link of each cell is 4400μF. The parameters of the system are summarized at Table 1.

TABLE I. Circuit Parameters and Experimental Condition

Description	Abbreviation	Value
Rated power	S_{MMC}	10kVA
DC-link voltage	V_{dc}	300V
Cell capacitor	C_{cell}	4400μF
Arm inductor	L	2mH
Switching frequency	f_{sw}	2kHz

The MMC was connected to drive 11kW 8-pole Permanent Magnet Synchronous Machine (PMSM) which is coupled to an Induction Machine (IM) for applying load torque to PMSM as shown like Fig. 5. The rated torque and speed of the PMSM are 60N-m and 1750r/min, respectively. The specification of PMSM is summarized at Table 2.

TABLE II. Specification of the PMSM

Description	Abbreviation	Value
Rated active power	P_{PMSM}	11kW
Rated line-to-line rms voltage	V_{rated}	200V
Rated rms line current	I_{rated}	58.6A
Rated rotational speed	ω_{rm}^{rated}	1750r/min
Pole pair number	pp	4

A. The Sinusoidal Leg Offset Voltage Injection

The Fig. 6 shows the waveform in condition of the low frequency mode with 1Hz output frequency. The injected leg offset voltage was 100Hz sinusoidal wave. Fig. 6 shows the upper and lower arm energies of *u*-phase from (10)-(11). The difference between upper and lower arm is counterbalanced by $\hat{v}_{sn}^{*}\hat{i}_{xo}^{*}$. When the difference of energies, E_{uP}-E_{uN}, is negative, the high frequency circulating current and offset voltage are controlled to be 180 degree out of phase as shown like Fig. 6(a). In contrast, when the difference is positive, the circulating current and offset voltages are controlled to be in phase as Fig. 6(b).

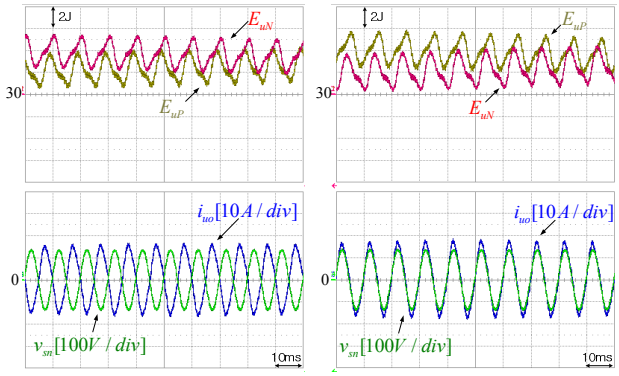

(a) (b)

Fig. 6. The waveform of the low frequency mode with 1Hz output frequency when using the sinusoidal leg offset voltage: (a) negative energy difference and (b) positive energy difference.

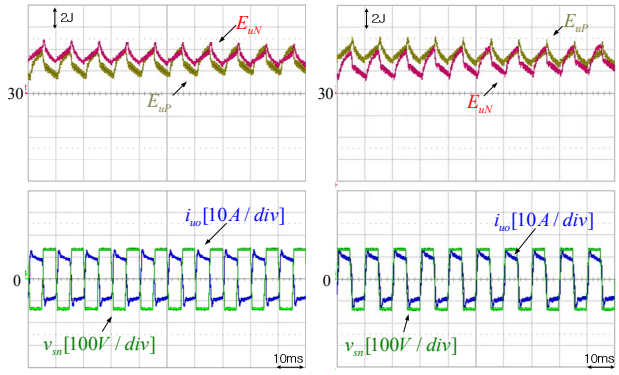

(a) (b)

Fig. 7. The waveform of the low frequency mode with 1Hz output frequency when using the square leg offset voltage: (a) negative energy difference and (b) positive energy difference.

B. *The Square Leg Offset Voltage Injection*

The Fig. 7 is the waveform of the low frequency mode with 1Hz output frequency. The balancing control is performed by using 100Hz square wave leg offset voltage. Fig. 7 shows the energies of upper and lower arm in u-phase leg. The difference of energy is counterbalanced by $v_{sn}^{*}i_{xo}$ like the preceding case of sinusoidal wave. In this experiment, the trapezoidal wave was used instead of square wave, because the output voltage might have unwanted high frequency distortion by the nonlinearities such as dead time when using the square wave. If the difference of energy, E_{uP}-E_{uN}, is negative, the high frequency circulating current and offset voltage are controlled to be 180 degree out of phase as shown like Fig. 7(a). In contrast, when the difference is positive, the circulating current and offset voltages are controlled to be in phase as Fig. 7(b).

As described in [7], the square wave can shave the peak of circulating current by 50%. However, because of trapezoidal waveform in this experiment the peak value of circulating current (i_{xo}) when using the trapezoidal leg offset voltage is smaller by 37% than that when using the sinusoidal voltage.

C. *Dynamic comparison between circulating current injection and leg offset voltage injection*

Fig. 8 shows the low frequency operation at 1Hz (15r/min), applying an abrupt step load torque from 0N-m to 24N-m (40%) at t_0. The square wave leg offset voltage was injected in 100Hz for the arm balancing at this experimental result. Before t_0, the PMSM was controlled to be 15r/min without load torque. At the time t_0, 40% step load torque is applied by torque control of the IM. After the time point, t_0, the fluctuations of upper and lower arm energy become larger because of the significant output phase current by the step load torque. Regardless of the impact of load torque, PMSM has successfully kept the speed showing reasonable low speed performance. This result confirms that the proposed controller achieves a good transient response.

In contrast, the conventional circulating current injection method has been applied to balancing control in this experiment as shown like Fig. 9. For comparison between the conventional current injection and the proposed leg offset voltage injection methods, the bandwidth for two methods was set as the same, and the frequency of the injected component was also set as the same, 100Hz. But the magnitude of the step load torque applied at the conventional current injection method was a half of the proposed method in Fig. 8. As shown in Fig. 9, the system became unstable and stalled at the end in spite of lower external load torque. After the abrupt step load torque was applied at t_0, the fluctuations of the upper and lower arm energies were larger than that when using leg offset voltage injection method in Fig. 8. Finally, the balancing controller could not accomplish the system balance, and then the overvoltage trip of cell capacitor was occurred and the system was stalled at the time point of t_1.

And it can be concluded that the leg offset voltage injection method reveals better disturbance load torque rejection performance.

D. *The Operation from Standstill to Normal Frequency Mode*

Finally, Fig. 10 shows the operation from standstill to the normal frequency mode, 1000*r/min*. In order to conduct the switchover operation in practical application of variable speed drive such as fans, blowers, or pumps, the load torque was applied in proportional to the square of the speed. Also, the startup torque of 24*N-m* (40%) is included in the torque profile. So, the phase current before t_{start} is regulated as DC value. At the time point t_{change}, the switchover process starts, and the operating mode changes to the normal frequency operation mode. When the rotating speed (ω_{rm}) is 1000r/min, the applied load torque to PMSM is 100% of the rated torque, 60N-m. As shown in Fig. 10, it has been confirmed that the proposed control strategies depicted in Fig. 4 were well implemented and incorporated properly to drive variable speed AC machine in overall speed including standstill by MMC.

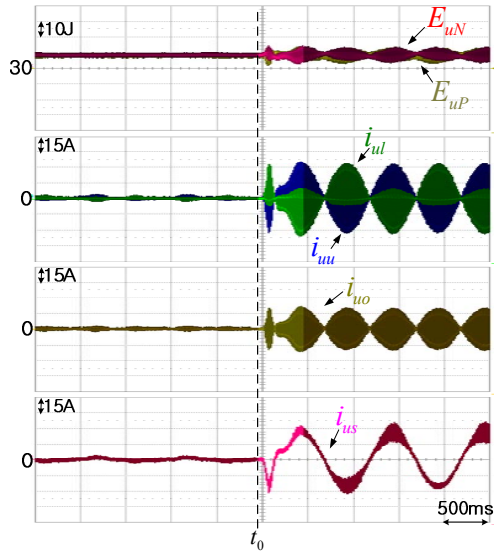

Fig. 8. The waveform when applying the leg offset voltage injecion method with $\omega_{rm} = 15\mathrm{r/min}$ and 40% step load torque at t_0.

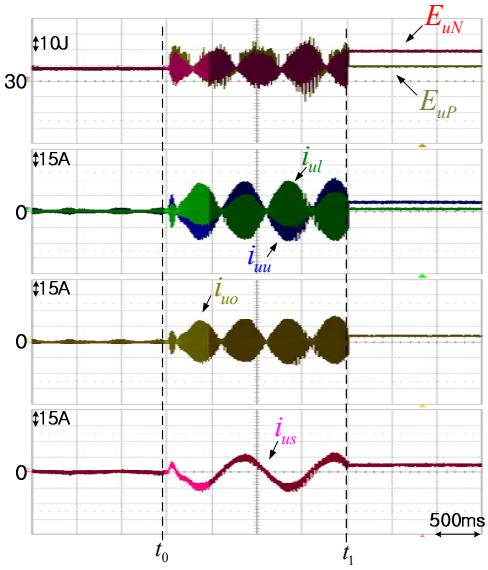

Fig. 9. The waveform when applying the conventional circulating current injecion method with $\omega_{rm} = 15\mathrm{r/min}$ and 20% step load torque at t_0.

VI. Conclusions

In this paper, a control strategy for variable-speed AC motor drives by the MMC has been presented. To overcome the difficulties of the power balance between cells and arms of MMC over wide operation speed range, the leg offset voltage injection method has been devised. With the proposed method, the ripple voltage of each cell of MMC has been kept within allowable bound under the sudden application of 40% of rated load torque at extremely low frequency, 1Hz, less than 1% of rated frequency. Based on the experimental results, it can be said that the control performance of the upper and lower arm energy ripple by the proposed leg offset voltage injection method, even though that has no inner circulating current regulation loop for arm energy balancing, is better than that by the conventional circulating current injection method. In addition, a variable speed AC motor drive in overall speed including standstill has also been verified by the experiments based on switchover tactic.

References

[1] Lesnicar, A., and R. Marquardt. "An innovative modular multilevel converter topology suitable for a wide power range." *Power Tech Conference Proceedings, 2003 IEEE Bologna*. Vol. 3. IEEE, 2003.

[2] Hiller, Marc, et al. "A new highly modular medium voltage converter topology for industrial drive applications." *Power Electronics and Applications, 2009. EPE'09. 13th European Conference on*. IEEE, 2009.

[3] Adam, Grain Philip, et al. "Modular multilevel inverter: pulse width modulation and capacitor balancing technique." *IET power electronics* 3.5 (2010): 702-715.

[4] Pirouz, H. Mohammadi, M. Tavakoli Bina, and K. Kanzi. "A new approach to the modulation and dc-link balancing strategy of modular multilevel ac/ac converters." *Power Electronics and Drives Systems, 2005. PEDS 2005. International Conference on*. Vol. 2. IEEE, 2005.

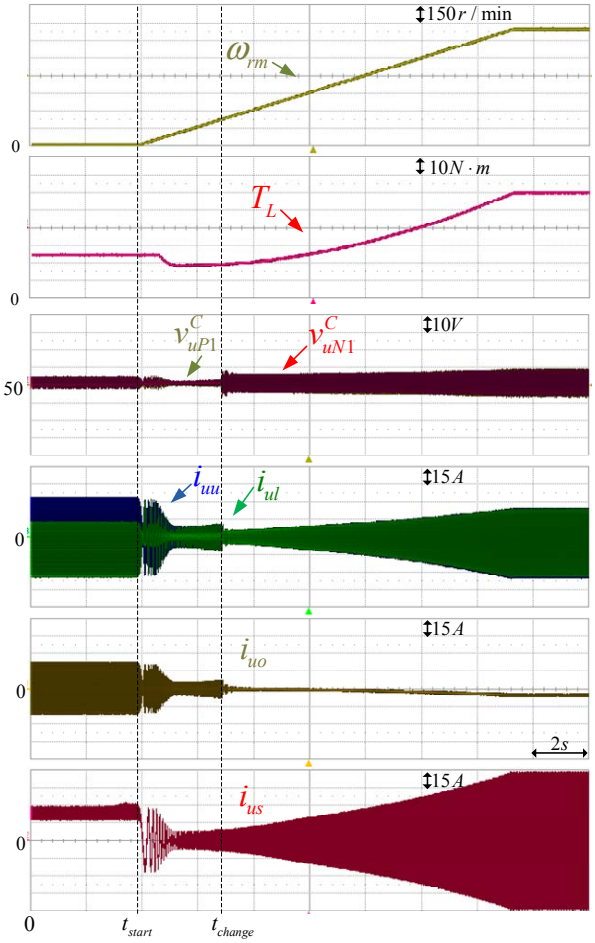

Fig. 10. Experimental waveforms in the condition of variable speed drive from starting to 1000r/min with 40% starting torque and the increasing load torque depending on rotating speed.

[5] Antonopoulos, Antonios, et al. "On interaction between internal converter dynamics and current control of high-performance high-power ac motor drives with modular multilevel converters." *Energy Conversion Congress and Exposition (ECCE), 2010 IEEE*. IEEE, 2010.

[6] Hagiwara, Makoto, Kazutoshi Nishimura, and Hirofumi Akagi. "A medium-voltage motor drive with a modular multilevel PWM inverter." *Power Electronics, IEEE Transactions on* 25.7 (2010): 1786-1799.

[7] Hagiwara, Makoto, Isamu Hasegawa, and Hirofumi Akagi. "Startup and low-speed operation of an adjustable-speed motor driven by a modular multilevel cascade inverter (MMCI)." *Energy Conversion Congress and Exposition (ECCE), 2012 IEEE*. IEEE, 2012.

[8] Kolb, Johannes, Felix Kammerer, and Michael Braun. "Straight forward vector control of the Modular Multilevel Converter for feeding three-phase machines over their complete frequency range." *IECON 2011-37th Annual Conference on IEEE Industrial Electronics Society*. IEEE, 2011.

[9] Antonopoulos, Antonios, et al. "Modular multilevel converter ac motor drives with constant torque form zero to nominal speed." *Energy Conversion Congress and Exposition (ECCE), 2012 IEEE*. IEEE, 2012.

[10] Jung, Jae-Jung, Hak-Jun Lee, and Seung-Ki Sul. "Control of the Modular Multilevel Converter for variable-speed drives." *Power Electronics, Drives and Energy Systems (PEDES), 2012 IEEE International Conference on*. IEEE, 2012.

[11] Angquist, Lennart, et al. "Inner control of modular multilevel converters-an approach using open-loop estimation of stored energy." *Power Electronics Conference (IPEC), 2010 International*. IEEE, 2010.

[12] Wang, Tengfei, and Yongqiang Zhu. "Analysis and comparison of multicarrier PWM schemes applied in H-bridge cascaded multi-level inverters." *Industrial Electronics and Applications (ICIEA), 2010 the 5th IEEE Conference on*. IEEE, 2010.

[13] Rohner, Steffen, et al. "Modulation, losses, and semiconductor requirements of modular multilevel converters." *Industrial Electronics, IEEE Transactions on*57.8 (2010): 2633-2642.